Kragujevac J. Sci. (2025) 47 (1) 5-29
doi: 10.5937/KgJSci2501005K

UDC 620.3:537.612:532.517
Original scientific paper

IMPACTS OF THE MOVING MAGNETIC FIELD ON THE SECOND-GRADE HYBRID NANOFLUID FLOW THROUGH A POROUS MATRIX IN A SYMMETRIC CHANNEL

Jitendra Kumar Singh*

Siddharth University Kapilvastu, Faculty of Science, Department of Mathematics, Siddharthnager-272202, India
*Corresponding author; E-mail:s.jitendrak@yahoo.com

(Received September 29, 2024; Accepted March 27, 2025)

ABSTRACT. The overwhelming applications of hydromagnetic flows of hybrid nanofluid and second-grade nanofluid in advanced nanotechnology and biomedical fields motivated this research work. This paper explores the heat transfer in unsteady hydromagnetic flows of Titanium Oxide-Copper Oxide-Engine Oil (TiO_2-CuO-EO) second-grade hybrid nanofluid in a uniform porous matrix bounded by two symmetrically placed vertical walls. The magnetic field applied strength is considered strong enough to generate Hall and ion-slip currents and is considered moving. The governing equations are obtained from the fundamental physical laws involved in the physical problem. An analytical approach is opted for solving the governing equations. The MATLAB computation of the solutions highlights the impressions of flow impacting parameters to the velocity, temperature, shear stress and rate of heat transport. Two special cases of interest are considered for the results analysis, namely, (a) the moving magnetic field, and (b) the stationary magnetic field. The study results infer that the static magnetic field employs the flow-suppressing force while the moving magnetic field employs the flow-boosting force in the flow field. In a static magnetic field, the velocity in the hybrid nanofluid is higher than the nanofluids. This behaviour is reversed in the moving magnetic field. The hybrid nanofluids are thermally more efficient than the nanofluids. In this study, it is noted that the rate of heat transfer at the left moving wall in the hybrid nanofluid is smaller than the nanofluid while at the right static wall, this effect is the opposite. This may be due to the fluctuation of wall temperature of the left-moving wall.
Mathematics Subject Classification: 76W05, 76R10, 76S05, 76U05.

Keywords: Second-grade fluid; hybrid nanofluid; porous matrix; moving magnetic field; Hall and ion-slip currents.

INTRODUCTION

The studies on nanofluid and hybrid nanofluid have continuously drawn the attention of the research fraternity due to their diverse applications in advanced cooling systems, energy-efficient heat exchangers, and biomedical devices, where their superior thermal

ORCID:
J. K. Singh: 0000-0002-7581-0564.

conductivity and stability offer advantages for optimizing thermal management and improving system efficiency. In a nanofluid, nanoparticles are suspended in a base fluid whereas in a hybrid nanofluid, the blends of different nanoparticles are suspended in the base fluid. They offer enhanced heat transfer capabilities, making them useful in diverse applications such as electronic cooling, solar energy systems, and biomedical devices. Stimulated by these applications ANJALI DEVI and SURIYA UMA DEVI (2016) discovered that the heat transfer rate of the hybrid nanofluid is higher than that of the nanofluid in a magnetic field environment and the heat transport rate can be further improvised by adding combinations of different nanocomposites. AFRIDI *et al.* (2019) explored that viscous dissipation causes the temperature increase of the hybrid nanofluids. KALAIVANAN *et al.* (2020) looked into the impact of Arrhenius activation energy on mass and heat transmission in second-grade nanofluid flow and found that activation energy augments the concertation profile. MUHAMMAD *et al.* (2021) and JAMSHED *et al.* (2021) discussed the dissipative effects of hybrid nanofluid fluid flow. In a recent study, LI *et al.* (2023) analysed the behaviour of a ternary nanofluid flowing over a stretching sheet. SHAH *et al.* (2024) applied the power law model to explore the heat transmission efficiency of the hybrid nanofluid flow over a stretching sheet. The second-grade fluids are a class of non-Newtonian fluids exhibiting complex rheological behaviours due to their elastic properties. The sophisticated modelling process of second-grade fluid flows makes it a prominent area of research. The second-grade fluid has significant industrial applications in the biochemical and petrochemical industries, food processing, etc. Motivated by the widespread applications SHAH and KHAN (2016), HAYAT *et al.* (2017), DAS and SAHOO (2018), JAVAID *et al.* (2020) studied the dynamics of second-grade fluid under diverse geometrical conditions. These researchers discovered that the non-Newtonian fluid employs more resistivity in the flow than the Newtonian fluid. In a recent research PUNITH GOWDA *et al.* (2021) observed that the Marangoni number significantly alters the temperature of the second order fluid. GUEDRI *et al.* (2022) applied the fractional kind of Newtonian heating to study the dynamics of second-grade fluid flow over an inclined plate. HUANG *et al.* (2022) implemented the fractional order Maxwell model to scrutinize the process of viscoelastic fluid flooding on the displacing oil. Most recently, SALAHUDDIN *et al.* (2022) and GULL *et al.* (2024) discussed the flow nature of viscoelastic fluid over a stretching sheet with temperature-dependent physical properties.

The mutual interaction of the electrically conducting fluid and the presence of an applied magnetic field result in the hydromagnetic phenomena. A pumping force and an electric field are generated from the hydromagnetic phenomena. The pumping force brings the rigidity in the flow velocity. If the strength of the applied magnetic field is strong and the diffusion velocity of electrons and ions are comparable, there arises the Hall and ion-slip currents from the electromagnetic phenomena. In the research, it is noted that these currents significantly alter the behaviour of the flow. The dynamics of electrically conducting fluid attracted the research community's attention since its inception of this area due to its tremendous applications in power generation systems, propulsion technology, boundary layer control, biomedicine for targeted drug delivery, and petroleum and agricultural engineering sectors. The stimulus of these facts, the dynamics of nanofluid and second-grade fluid are studied in the appearance of magnetic field domain. The hydromagnetic effects on second-grade fluid flow under diverse geometrical setups and methodologies have recently been explored by several authors, namely, SINGH *et al.* (2018, 2020), SINGH and VISHWANATH (2020), HAQ *et al.* (2021), SINGH and SETH (2022), KUMAR *et al.* (2022), HOSSEINZADEH *et al.* (2023) and SEHRA *et al.* (2023). The heat transport behaviour of nanofluids/ hybrid nanofluids flow in the magnetic field domain taking different physical aspects of the problems is considered by many research scientists: SRINIVASA *et al.* (2019), SHEIKHOLESLAMI *et al.* (2019), SRAVAN KUMAR *et al.* (2020), SINGH and KOLASANI (2021), BASHIR *et al.* (2021), KHAN *et al.* (2022), HUSSAIN *et al.* (2022, 2023), ABBAS *et al.* (2023), SINGH *et al.* (2023a,

2023b, 2023c), SHAH *et al.* (2024). More recently, SAKTHI *et al.* (2024a, 2024b) and ENAMUL and ONTELA (2024) examined the flow characteristics of the second-grade hybrid nanofluid flow under diverse physical and geometrical conditions. SINGH *et al.* (2024) considered the Hall current and thermo diffusion impacts on heat and mass transport of MHD nanofluid flow over a magnetized surface.

The heat transport in unsteady second-grade hybrid nanofluid flow in a vertical channel bounding the porous matrix in the presence of a moving magnetic field has not yet been explored by any researcher. To fill this gap, the study of the heat transport in oscillatory hydromagnetic second-grade hybrid nanofluid flow in a vertical channel with a moving applied magnetic field is performed in this paper. It is considered that the applied magnetic field is moving with the velocity $K_1 u_0 f(t) = K_1 u_0 (1 + \varepsilon \cos(\omega t))$. When $K_1 = 1$, the applied magnetic field is fixed relative to the left moving wall whereas when $K_1 = 0$, the applied magnetic field is static. The originality of this research work is

(I) the consequence of wall movement on the flow characteristics,

(II) the impact of second-grade parameters and volume concentration of nanofluids.

The mathematical model of the flow problem is solved analytically. The MATLAB computation of the solutions highlights the impressions of flow-impacting parameters on the nature of the flow. It is witnessed that the static magnetic field employs the flow-suppressing force while the moving magnetic field employs the flow-boosting force in the flow field.

Illustration of physical problem and governing equations

The physical problem considers the laminar unsteady flow of incompressible thermally and electrically conducting TiO_2-CuO-EO second-grade hybrid nanofluid in a porous matrix bounded within a symmetrical vertical channel in a moving strong magnetic field domain. The geometrical setup of the problem is illustrated in Figure 1.

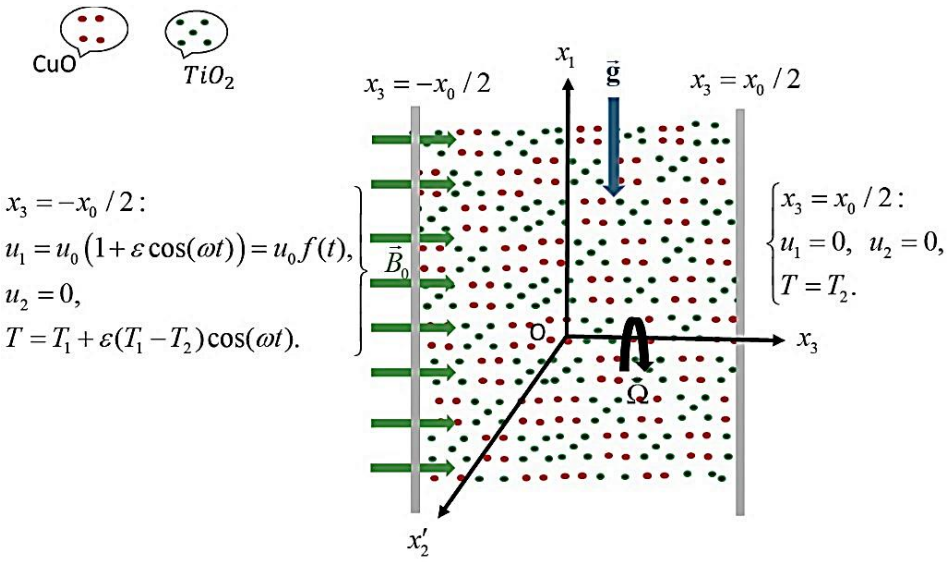

Figure 1. Geometrical setup of the problem.

Undertaking the following flow conditions for the derivation of the mathematical model of the physical problem:

(a) The second-grade hybrid nanofluid is dilute.

(b) For the incompressible homogeneous second-grade fluid, the Cauchy stress tensor is given as (RIVILIN and ERICKSEN, 1955)

$$\left.\begin{aligned}
&\vec{T} = -p\vec{I} + \mu_{hnf}\vec{A}_1 + \alpha_1\vec{A}_2 + \alpha_1\left(\vec{A}_1\right)^2,\\
&\vec{A}_1 = \nabla\vec{u} + \left(\nabla\vec{u}\right)^T,\\
&\vec{A}_2 = \frac{\partial\vec{A}_1}{\partial t} + \left(\vec{u}\cdot\nabla\right)\vec{A}_1 + \vec{A}_1\left(\nabla\vec{u}\right) + \left(\nabla\vec{u}\right)^T\vec{A}_1.
\end{aligned}\right\} \tag{1}$$

(c) The Darcy-Brinkman model for the flow through the porous matrix is undertaken which considers that the effective viscosity of the fluid is the same as the viscosity of the porous matrix i.e.

$$\nabla p = \mu_{hnf}\nabla^2\vec{u} - \frac{\mu_{hnf}\vec{u}}{k_p}. \tag{2}$$

(d) The applied magnetic field is considered strong, and the diffusion velocity of ions is comparable to that of electrons, thus the Hall and ion-slip currents are taken into account. The mathematical form of Ohm's law with Hall and ion-slip currents is (CRAMER and PAI, 1973)

$$\vec{j} + \frac{b_e}{\vec{B}_0}\left(\vec{j}\times\vec{B}\right) - \frac{b_e b_i}{\vec{B}_0}\left(\vec{j}\times\vec{B}\right)\times\vec{B} = \sigma_{hnf}\left(\vec{e} + \vec{u}\times\vec{B}\right). \tag{3}$$

(e) The motion-generated magnetic field is not taken into consideration because magnetic diffusion is sufficiently large in comparison to magnetic advection. The applied magnetic field moves with the velocity $K_1 u_0 f(t)$. Here $K_1 = 0$ when the magnetic field is stationary while $K_1 = 1$ when the velocity of the magnetic field and the moving left wall of the channel are the same and along $x_1 -$ direction.

(f) The gravitational effect on the flow in terms of the buoyancy force is considered via the Boussinesq approximation as

$$\vec{F}_b = \left(\rho\beta\right)_{hnf}\vec{g}(T - T_2). \tag{4}$$

The equations for motion (linear momentum and energy equations) under the aforementioned presumptions are

$$\rho_{hnf}\left(\frac{\partial u_1}{\partial t} - 2\Omega u_2\right) = \mu_{hnf}\left(\frac{\partial^2 u_1}{\partial x_3^2} - \frac{u_1}{k_p}\right) + \beta_\lambda\frac{\partial^3 u_1}{\partial x_3^2\partial t} - \frac{\sigma_{hnf}B_0^2}{(a_e^2 + b_e^2)}\left(a_e u_1 - b_e u_2 - K_1 u_0 f(t)\right)$$
$$+ g(\rho\beta)_{hnf}(T - T_2), \tag{5}$$

$$\rho_{hnf}\left(\frac{\partial u_2}{\partial t} + 2\Omega u_1\right) = \mu_{hnf}\left(\frac{\partial^2 u_2}{\partial x_3^2} - \frac{u_2}{k_p}\right) + \beta_\lambda\frac{\partial^3 u_2}{\partial x_3^2\partial t} - \frac{\sigma_{hnf}B_0^2}{(a_e^2 + b_e^2)}\left(b_e u_1 + a_e u_2\right), \tag{6}$$

$$\left(\rho C_p\right)_{hnf}\frac{\partial T}{\partial t} = k_{hnf}\frac{\partial^2 T}{\partial x_3^2} - S(T - T_2), \tag{7}$$

where $a_e = 1 + b_e b_i$.

The boundary conditions (BCs) at the symmetrically placed vertical walls of the channel are

$$u_1 = u_0(1+\varepsilon\cos(\omega t)),\ u_2 = 0,\ \ T = T_1 + \varepsilon(T_1 - T_2)\cos(\omega t), \qquad \text{at } x_3 = -x_0/2$$
$$u_1 = 0,\ u_2 = 0,\ \ T = T_2, \qquad \text{at } x_3 = x_0/2. \tag{8}$$

The mathematical form for the thermophysical conduct of the hybrid nanofluids is tabulated in Table 1.

Table 1. The mathematical form of various thermophysical conduct of the hybrid nanofluids (RANA *et al.*, 2021; BHATTI *et al.*, 2022).

Thermophysical Properties	Mathematical expression
Dynamic viscosity	$\frac{\mu_{hnf}}{\mu_f} = \frac{1}{(1-\phi_1)^{2.5}(1-\phi_2)^{2.5}} = \delta_1$
Density	$\frac{\rho_{hnf}}{\rho_f} = (1-\phi_2)\left[(1-\phi_1) + \phi_1\frac{\rho_{s_1}}{\rho_f}\right] + \phi_2\frac{\rho_{s_2}}{\rho_f} = \delta_2$
Thermal expansion coefficient	$\frac{(\rho\beta)_{hnf}}{(\rho\beta)_f} = (1-\phi_2)\left[(1-\phi_1) + \phi_1\frac{(\rho\beta)_{s_1}}{(\rho\beta)_f}\right] + \phi_2\frac{(\rho\beta)_{s_2}}{(\rho\beta)_f} = \delta_3$
Electrical conductivity	$\frac{\sigma_{nf}}{\sigma_f} = \frac{\sigma_{s_1}(1+2\phi_1) + 2\sigma_f(1-\phi_1)}{\sigma_{s_1}(1-\phi_1) + \sigma_f(2+\phi_1)} = \delta_4,$ $\frac{\sigma_{hnf}}{\sigma_f} = \frac{\sigma_{s_2}(1+2\phi_2) + 2\delta_4\sigma_f(1-\phi_2)}{\sigma_{s_2}(1-\phi_2) + \delta_4\sigma_f(2+\phi_2)} = \delta_4\delta_5$
Thermal conductivity	$\frac{k_{nf}}{k_f} = \frac{(k_{s_1}+2k_f) + 2\phi_1(k_{s_1}-k_f)}{(k_{s_1}+2k_f) - \phi_1(k_{s_1}-k_f)} = \delta_6,$ $\frac{k_{hnf}}{k_f} = \frac{(k_{s_2}+2\delta_6 k_f) + 2\phi_2(k_{s_2}-\delta_6 k_f)}{(k_{s_2}+2\delta_6 k_f) - \phi_2(k_{s_2}-\delta_6 k_f)} = \delta_6\delta_7$
Heat capacity	$\frac{(\rho C_p)_{hnf}}{(\rho C_p)_f} = (1-\phi_2)\left[(1-\phi_1) + \phi_1\frac{(\rho C_p)_{s_1}}{(\rho C_p)_f}\right] + \phi_2\frac{(\rho C_p)_{s_2}}{(\rho C_p)_f} = \delta_8$
where $\delta_1, \delta_2, \delta_3, \delta_4, \delta_5, \delta_6, \delta_7$ and δ_8 **are thermophysical constants.**	

Table 2 The values of thermophysical constants TiO_2-CuO-EO (unused) (BHATTI *et al.*, 2022; SREEDEVI *et al.*, 2022; KOTHANDARAMAN and SUBRAMANYAN, 2010).

Thermophysical Constants (293K/20° C)	$\beta\times10^{-6}(1/K)$	$\rho(kg/m^3)$	$\sigma(S/m)$	$C_p(J/kgK)$	$k(W/mK)$
Titanium Oxide (TiO_2)	9	4250	2.38×10^{6}	686.2	8.9538
Copper Oxide (CuO)	18	6320	6.9×10^{-2}	531.8	76.5
Engine Oil (EO)	700	884	700	1910	0.144

A non-dimensional mathematical model of the problem is attained with the assistance of the following transformations:

$$X_3 = \frac{x_3}{x_0},\ U_1 = \frac{u_1}{u_0},\ U_2 = \frac{u_2}{u_0},\ \tau = \frac{tu_0}{x_0},\ n = \frac{\omega x_0}{u_0},\ \Theta = \frac{T-T_2}{T_1-T_2}. \tag{9}$$

Employing the transformations defined in equation (9) and mathematical expressions of the thermophysical nature of the hybrid nanofluids in equations (5) to (8), yields

$$\mathrm{Re}\frac{\partial}{\partial\tau}\left(\delta_2 U-\beta_\lambda^*\frac{\partial^2 U}{\partial X_3^2}\right)-\delta_2\frac{\partial^2 U}{\partial X_3^2}+\lambda_1 U=\lambda_2 f(\tau)+\delta_3 G_\Theta\Theta, \tag{10}$$

$$\delta_8\,\mathrm{Re}\,\mathrm{Pr}\frac{\partial\Theta}{\partial\tau}=\delta_6\delta_7\frac{\partial^2\Theta}{\partial X_3^2}-S\Theta, \tag{11}$$

where

$$\upsilon_f=\frac{\mu_f}{\rho_f},\ \mathrm{Re}=\frac{u_0x_0}{\upsilon_f},\ Ro=\frac{\Omega x_0^2}{\upsilon_f},\ \beta_\lambda^*=\frac{\beta_\lambda}{\rho_f x_0^2},\ Ha^2=\frac{\sigma_f x_0^2B_0^2}{\mu_f},$$

$$K_p=\frac{k_p}{x_0^2},\ G_\Theta=\frac{g\beta_f x_0^2(T_1-T_2)}{\upsilon_f u_0},\ \mathrm{Pr}=\left(\frac{\upsilon\rho C_p}{k}\right)_f,\ S_1=\frac{Sx_0^2}{k_f},$$

$$\lambda_1=\frac{\delta_1}{K_p}+2i\delta_2 Ro+\frac{\delta_4\delta_5 Ha^2(a_e+ib_e)}{(a_e^2+b_e^2)},\ \lambda_2=\frac{\delta_4\delta_5 Ha^2K_1}{(a_e^2+b_e^2)},\ U=U_1+iU_2.$$

The BCs in dimensionless form become

$$\begin{aligned}&U=1+\varepsilon\cos(n\tau),\ \Theta=1+\varepsilon\cos(n\tau), && \text{at } X_3=-1/2\\ &U=0,\ \Theta=0), && \text{at } X_3=1/2.\end{aligned} \tag{12}$$

Solution method of the problem

Due to the oscillatory nature of the fluid properties on the boundary walls, we may assume the following forms of the solutions for the velocity and temperature

$$U(X_3,\tau)=U_{s1}(X_3)+\left(\varepsilon/2\right)\left(U_{s2}(X_3)e^{i\omega\tau}+U_{s3}(X_3)e^{-i\omega\tau}\right), \tag{13}$$

$$\Theta(X_3,\tau)=\Theta_{s1}(X_3)+\left(\varepsilon/2\right)\left(\Theta_{s2}(X_3)e^{i\omega\tau}+\Theta_{s3}(X_3)e^{-i\omega\tau}\right). \tag{14}$$

Use of the equations (13) and (14) to the resulting mathematical model of the problem (10) and (11) and the BCs (12) give

$$\delta_1\frac{d^2U_{s1}}{dX_3^2}-\lambda_1U_{s1}=-\lambda_2-\delta_3G_\Theta\Theta_{s1}, \tag{15}$$

$$\left(\delta_1\pm in\beta_\lambda^*\,\mathrm{Re}\right)\frac{d^2U_{si}}{dX_3^2}-\left(\lambda_1\pm in\delta_2\,\mathrm{Re}\right)\lambda_1U_{si}=-\lambda_2-\delta_3G_\Theta\Theta, \tag{16}$$

$$\delta_6\delta_7\frac{d^2\Theta_{s1}}{dX_3^2}-S_1\Theta_{s1}=0, \tag{17}$$

$$\delta_6\delta_7\frac{d^2\Theta_{si}}{dX_3^2}-\left(S_1\pm in\delta_8\,\mathrm{Re}\,\mathrm{Pr}\right)\Theta_{si}=0. \tag{18}$$

The ‘+ive’ and ‘-ive’ signs in the equations (16) and (18) appearing for the suffix $i=2$ and $i=3$ respectively.

The BCs after utilizing of equations (13) and (14) yields

$$\begin{aligned}&U_{si}=1,\ \Theta_{si}=1, && \text{at } X_3=-1/2\\ &U_{si}=0,\ \Theta_{si}=0, && \text{at } X_3=1/2,\quad i=1,2,3.\end{aligned} \tag{19}$$

Solving equations (15) to (18) together with boundary circumstances (19), we obtain

$$U_{s1} = -\frac{\sinh\left(\beta_1(X_3-(1/2))\right)}{\sinh\left(\beta_1\right)} + \frac{\lambda_2}{\lambda_1}\left[1-\frac{\cosh(\beta_1 X_3)}{\cosh\left(\beta_1/2\right)}\right] - \frac{\delta_3 G_\Theta}{\delta_1(\gamma_1^2-\beta_1^2)}\left[\frac{\sinh\left(\beta_1(X_3-(1/2))\right)}{\sinh\left(\beta_1\right)} - \frac{\sinh\left(\gamma_1(X_3-(1/2))\right)}{\sinh\left(\gamma_1\right)}\right], \tag{20}$$

$$U_{si} = -\frac{\sinh\left(\beta_i(X_3-(1/2))\right)}{\sinh\left(\beta_i\right)} + \frac{\lambda_2}{(\lambda_1 \pm in\delta_2\,\mathrm{Re})}\left[1-\frac{\cosh(\beta_i X_3)}{\cosh\left(\beta_i/2\right)}\right] - \frac{\delta_3 G_\Theta}{(\delta_1 \pm in\beta_\lambda^*\,\mathrm{Re})(\gamma_i^2-\beta_i^2)}\left[\frac{\sinh\left(\beta_i(X_3-(1/2))\right)}{\sinh\left(\beta_i\right)} - \frac{\sinh\left(\gamma_i(X_3-(1/2))\right)}{\sinh\left(\gamma_i\right)}\right], \quad i=2,3. \tag{21}$$

$$\Theta_{si} = -\frac{\sinh\left(\gamma_i(X_3-(1/2))\right)}{\sinh\left(\gamma_i\right)},\ i=1,\ 2,\ 3. \tag{22}$$

Where

$$\gamma_1 = \sqrt{\frac{S}{\delta_6\delta_7}},\ \gamma_{2,3} = \sqrt{\frac{S \pm in\delta_8\,\mathrm{Re}\,\mathrm{Pr}}{\delta_6\delta_7}},\ \beta_1 = \sqrt{\frac{\lambda_1}{\delta_1}},\ \beta_{2,3} = \sqrt{\frac{\lambda_1 \pm in\delta_2\,\mathrm{Re}}{\delta_1 \pm in\beta_\lambda^*\,\mathrm{Re}}}.$$

The '+ive' and '-ive' signs in the equation (22) are for $i=2$ and $i=3$ respectively. Implementing the solutions (20) to (22) in the equations, the closed-form solutions of the velocity and temperature are obtained. The quantities of the physical interest such as the shear stress and rate of heat transport are computed from the MATLAB computation of the closed-form solutions for velocity and temperature.

RESULTS

The MATLAB computation of the closed-form solutions explores the significant flow parameter's impact on the behaviour of the flow. The results of the velocity and temperature are exhibited in Figures 2 to 10 while the results of shear stress are explored in Figures 11 to 18. The rate of heat transmission is shown in Figure 19. The range of the parameter values used for the computation of the results is presented in Table 3.

The results for the velocity and temperature

The results of the velocity and temperature expressing the impact of different parameters are presented in Figures 2 to 10. Figure 2 discovers, that in a stationary magnetic field, the second-grade parameter produces rigidity in the main flow. In a moving magnetic it employs the flow-assisting force which causes the enhancement in the main flow. In general, the second-grade parameter lessens the main flow as in the case of the stationary magnetic field. Its behaviour is opposite in the moving magnetic field; this may be due to the movement of the magnetic field. The second-grade parameter assists the normal flow as seen in Figure 2.

Table 3. The range of the parameter values used for the computation of results (SINGH and VISHWANATH, 2020; SINGH *et al.*, 2023b, 2023c).

Parameter	Range	Fixed Value
β_λ^*	$0.15 \le \beta_\lambda^* \le 0.35$	$\beta_\lambda^* = 0.25$
$\phi_1,\ \phi_2$	$0 \le \phi_1,\ \phi_2 \le 0.02$	$\phi_1,\ \phi_2 = 0.02$
n	$1 \le n \le 3$	$n = 2$
Re	$1 \le \mathrm{Re} \le 3$	$\mathrm{Re} = 3$
Ro	$1 \le Ro \le 3$	$Ro = 3$
K_p	$0.05 \le K_p \le 2.0$	$K_p = 0.3$
Ha^2	$9 \le Ha^2 \le 25$	$Ha^2 = 25$
b_i	$0.5 \le b_i \le 2$	$b_i = 0.5$
b_e	$0.25 \le b_e \le 0.75$	$b_e = 0.5$
Pr	--	$\mathrm{Pr} = 5.2$
S_1	--	$S_1 = 2$

Further, it is seen that the flow velocity in the moving magnetic field is higher than in the stationary magnetic field. This implies that the flow-resisting force (Lorentz force) applied by the moving magnetic field on the flow field is less than that of the stationary magnetic field. The consequences of the volume concentration of hybrid nanofluid and nanofluid on velocity and temperature are presented in Figure 3. In the case of the static magnetic field, the velocity when $\phi_1 = 0.02,\ \phi_2 = 0.02$ is higher than when $\phi_1 = 0,\ \phi_2 = 0.02$, and $\phi_1 = 0.02,\ \phi_2 = 0$ i.e. the velocity in the TiO_2-CuO-EO hybrid nanofluid is higher than the CuO-EO and TiO_2-EO nanofluids. In the moving magnetic field this nature is reverse. The temperature when $\phi_1 = 0.02,\ \phi_2 = 0.02$ (TiO_2-CuO-EO hybrid nanofluid) is higher than when $\phi_1 = 0.02,\ \phi_2 = 0$, and $\phi_1 = 0,\ \phi_2 = 0.02$ (TiO_2-EO and CuO-EO nanofluids). This means that the dispersion of two different kinds of nanoparticles in a base fluid enhances the velocity and temperature of the fluid. This indicates that the hybrid nanofluids are more thermally efficient than the nanofluids. The flowing nature of fluid for the frequency of oscillations in Figure 4 emphasizes that the oscillations stabilize the main flow in the case of the static magnetic field while destabilizing it in the case of the moving magnetic field. This nature is because the oscillation frequency of the moving magnetic field is the same as that of the moving wall of the channel. The normal flow is destabilized by the frequency in the case of both the moving and the static magnetic field. The temperature near the left wall grows while within the remaining part of the channel reduces with the frequency. Usually, the motion of the wall of the channel destabilizes the flow in its vicinity which may cause the enhancement of temperature near the left wall. Figure 5 measures the influence of the Reynold number Re. The enhancement in the velocity is seen for the increasing Re values except on the main flow in the case of the static magnetic field. Incrementing Re values reduce the viscosity causing the growth in the fluid velocity. The effect Re value on the main is opposite because of the movement of the left wall of the channel. The temperature of the fluid lessens with the Re values except adjacent to the left moving wall. The enhancement in viscosity (reduction in Re values) causes more heat generation. This effect near the left wall is opposite due to the motion of the left wall. Figure 6 exhibits that rotation exerts a flow-stabilizing force on the main flow while it exerts a flow-destabilizing force on the normal flow. The rotation of the fluid exerts two forces Centripetal force and Coriolis force. The centripetal force acts in the

direction of the main flow and controls the main flow while the Coriolis force acts in the direction normal to the main flow and destabilizes the normal flow.

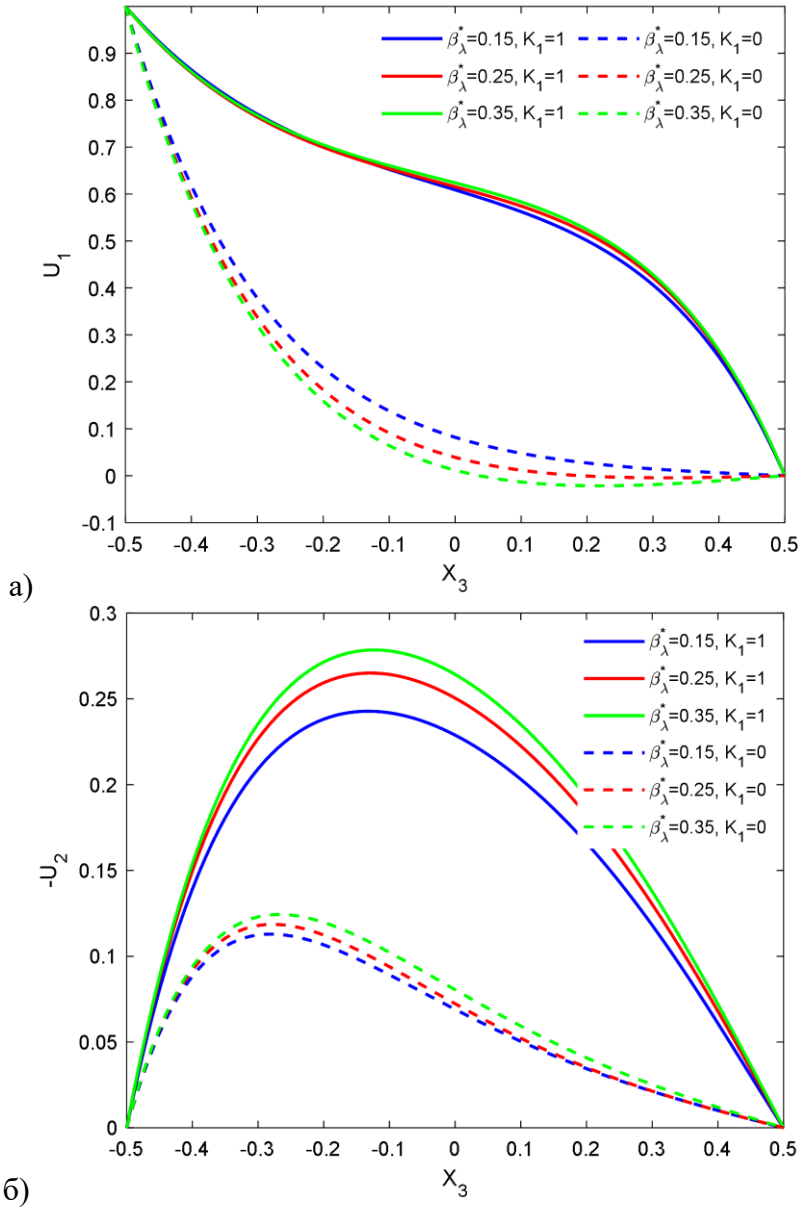

Figure 2. The effect of the second-grade parameter (β_λ^*) on the (a) main flow, (b) normal flow.

The results in Figure 7 expose that the increment in the permeability of the porous matrix leads to augmenting the velocity because the large permeability of the porous matrix produces less Darcian drag force. The effects of the applied magnetic field on the velocity are presented in Figure 8. This figure illustrates that the static magnetic field suppresses the flow velocity while the moving magnetic field boosts the velocity except close to the moving left wall. The electromagnetic force brings rigidity to the flow as the result shows for the static magnetic field. The moving magnetic field effect is contrary due to its movement. Figures 9 and 10 depict that the Hall and ion-slip currents diminish the main flow in a static magnetic field while in a moving magnetic field, this behaviour is contrary. Both the Hall and ion-slip currents accelerate the normal flow velocity because the origination of these currents is due to the revolution of fluid particles around the lines of an applied magnetic field.

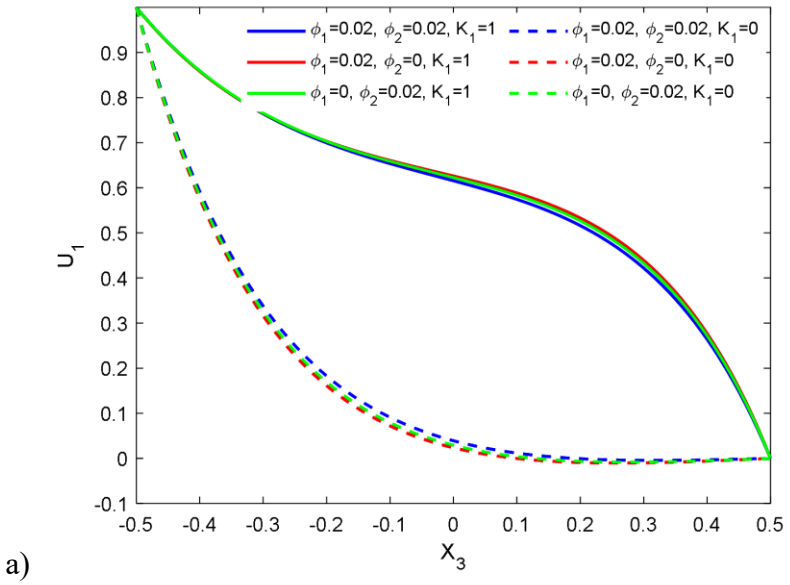

a)

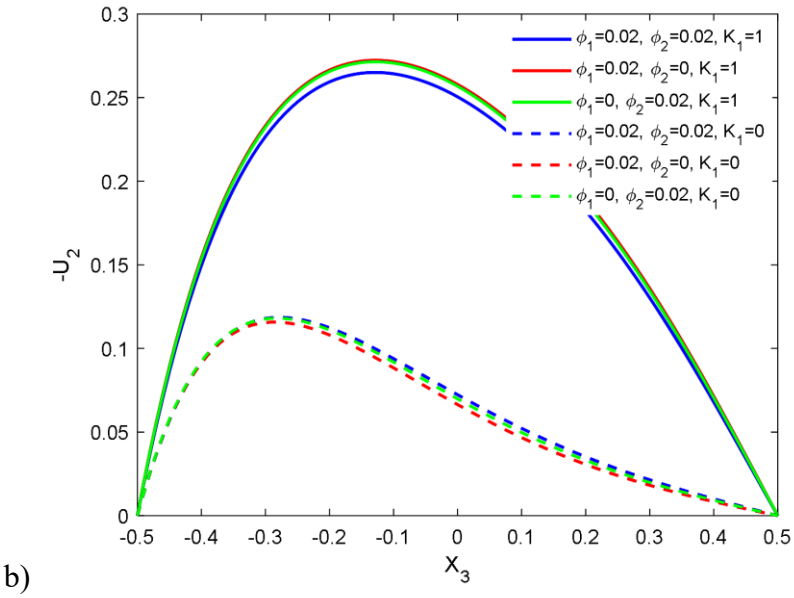

b)

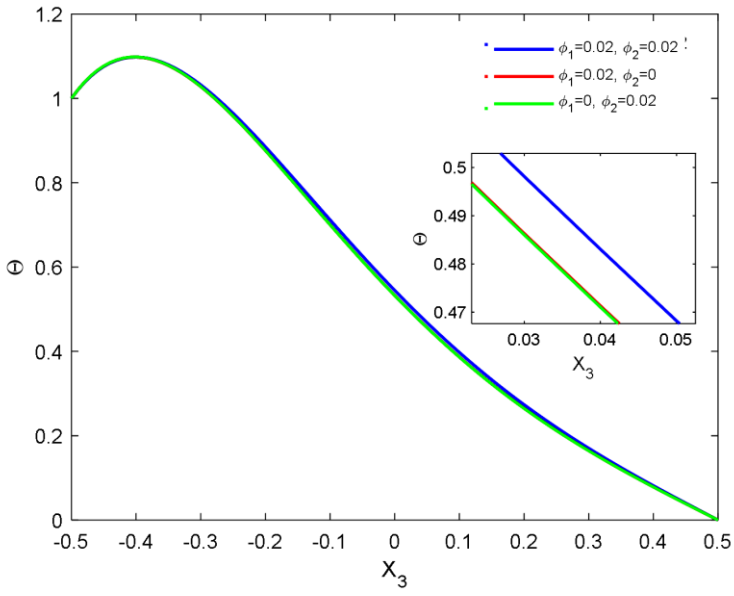

c)

Figure 3. The effect of volume concentrations (ϕ_1 and ϕ_2) on the (a) main flow, (b) normal flow and (c) temperature.

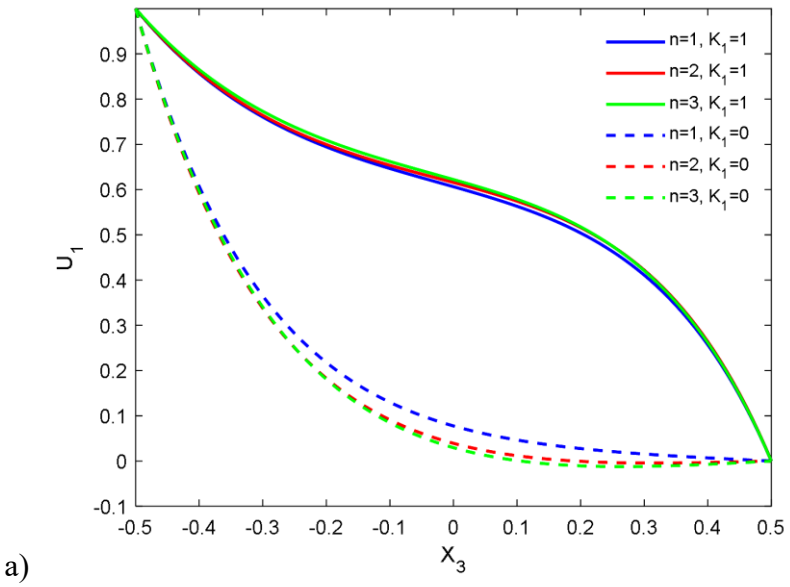

a)

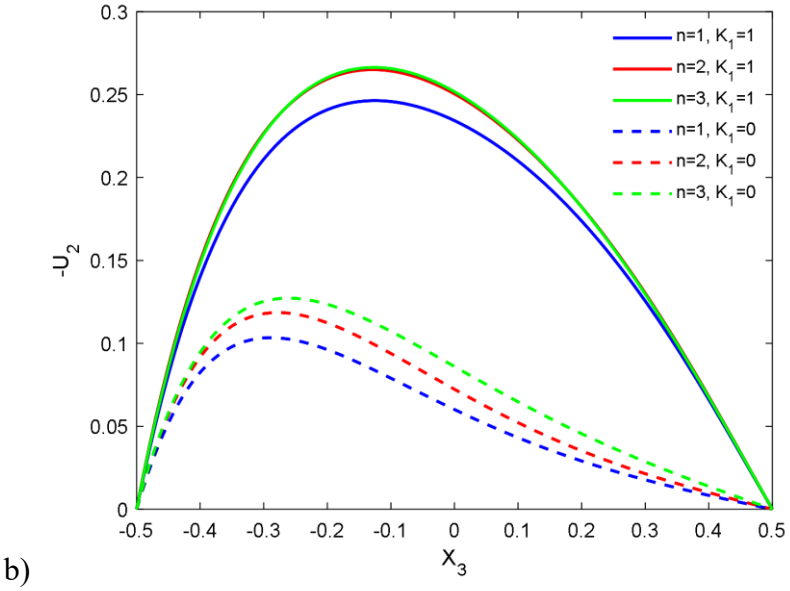

b)

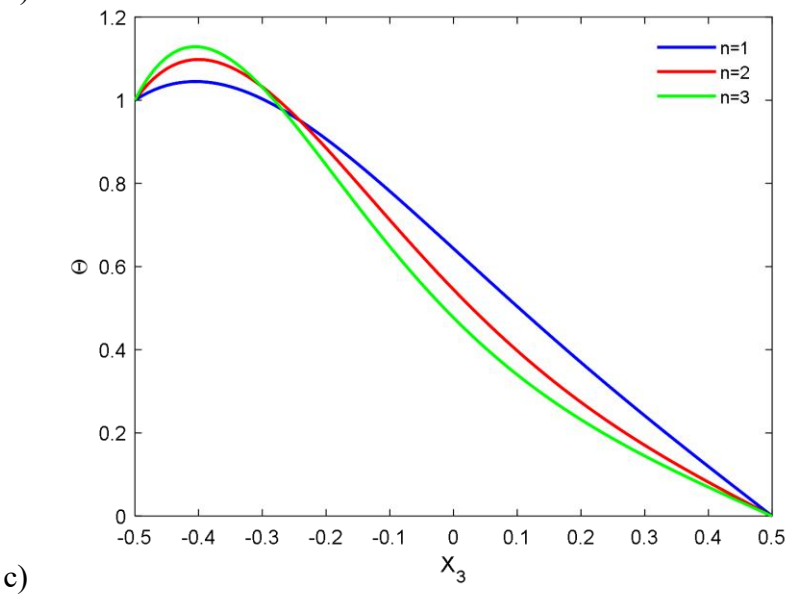

c)

Figure 4. The effect of frequency parameter (n) on the (a) main flow, (b) normal flow, and (c) temperature.

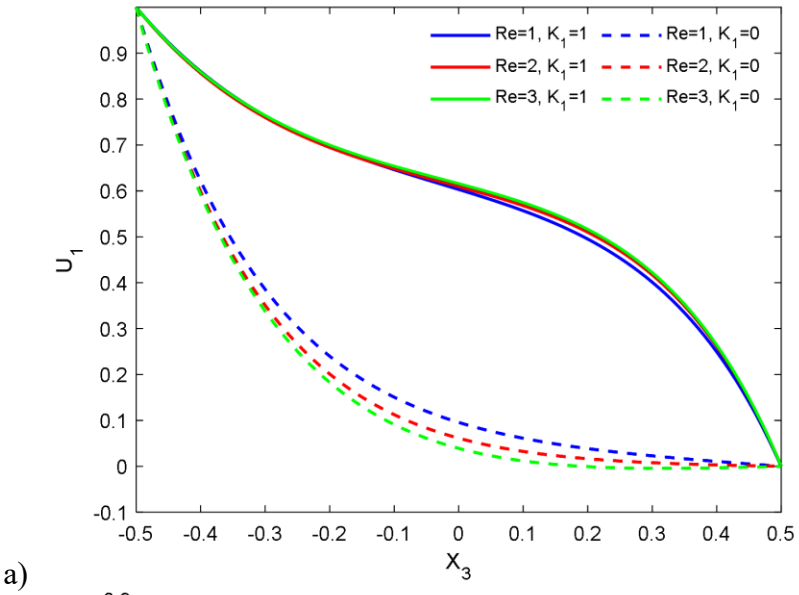

a)

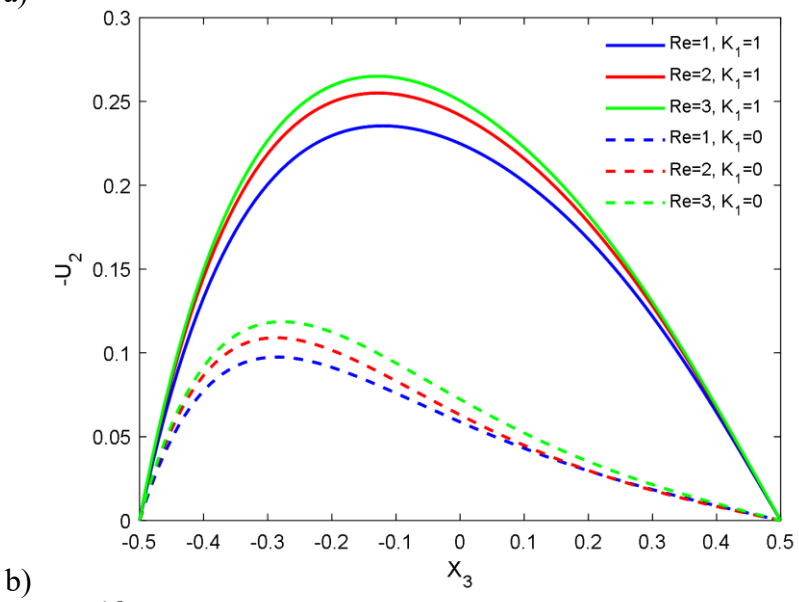

b)

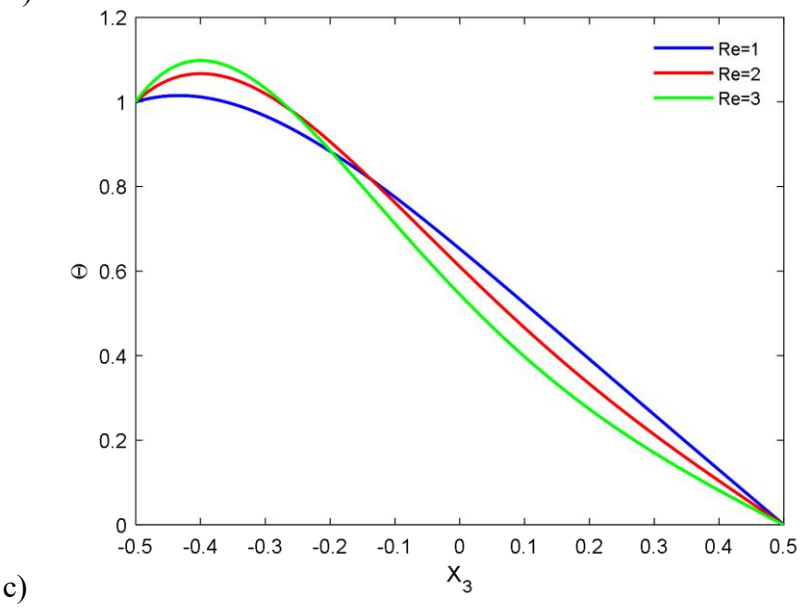

c)

Figure 5. The effect of Reynolds number (Re) on the (a) main flow, (b) normal flow, and (c) temperature.

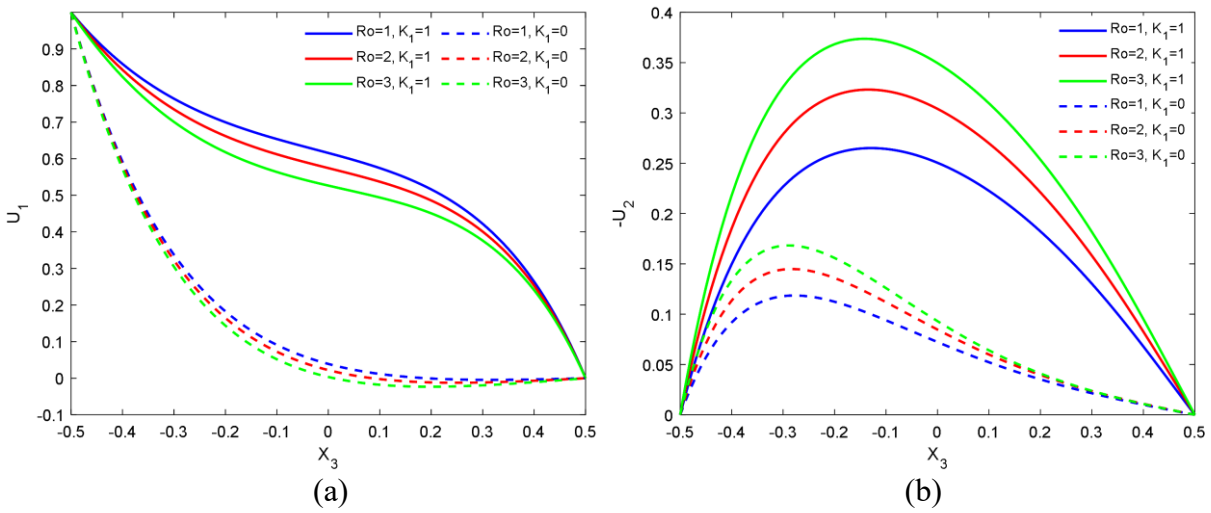

Figure 6. The effect of rotation (Ro) on the (a) main flow, (b) normal flow.

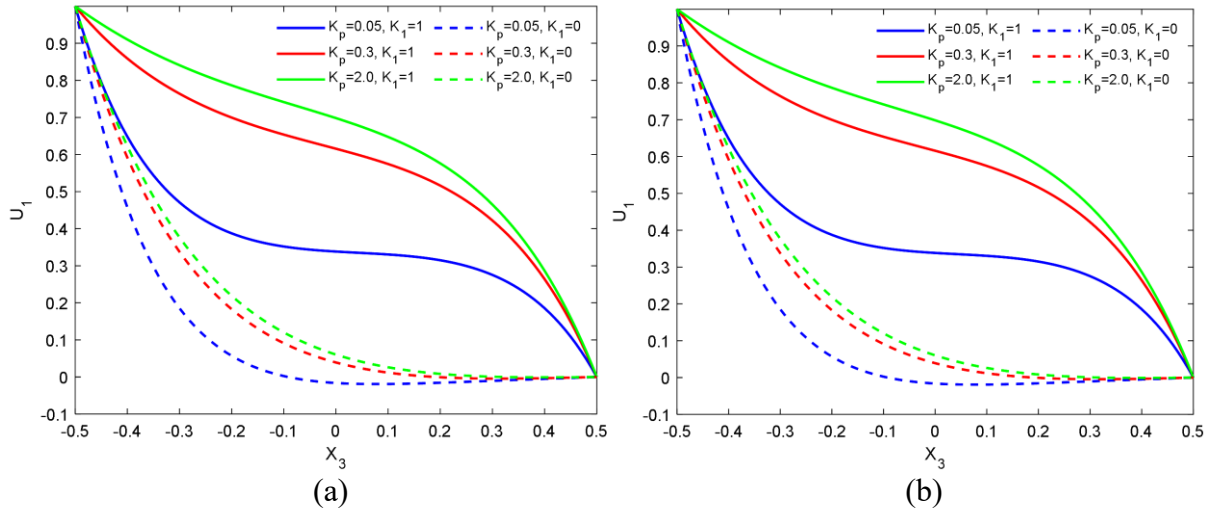

Figure 7. The effect of the permeability parameter (K_p) on the (a) main flow, (b) normal flow.

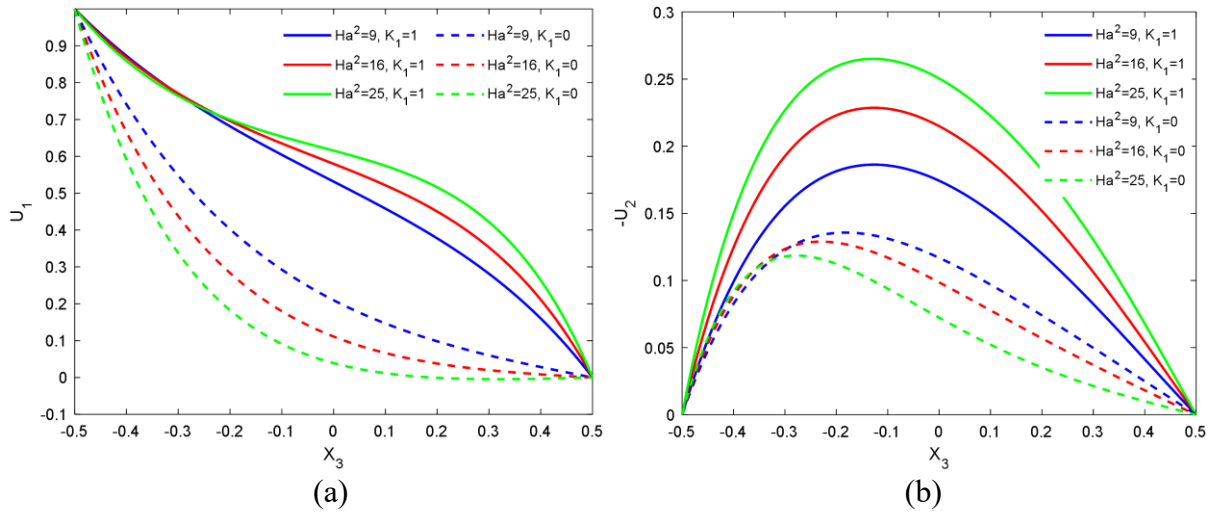

Figure 8. The effect of the magnetic parameter (Ha^2) on the (a) main flow, (b) normal flow.

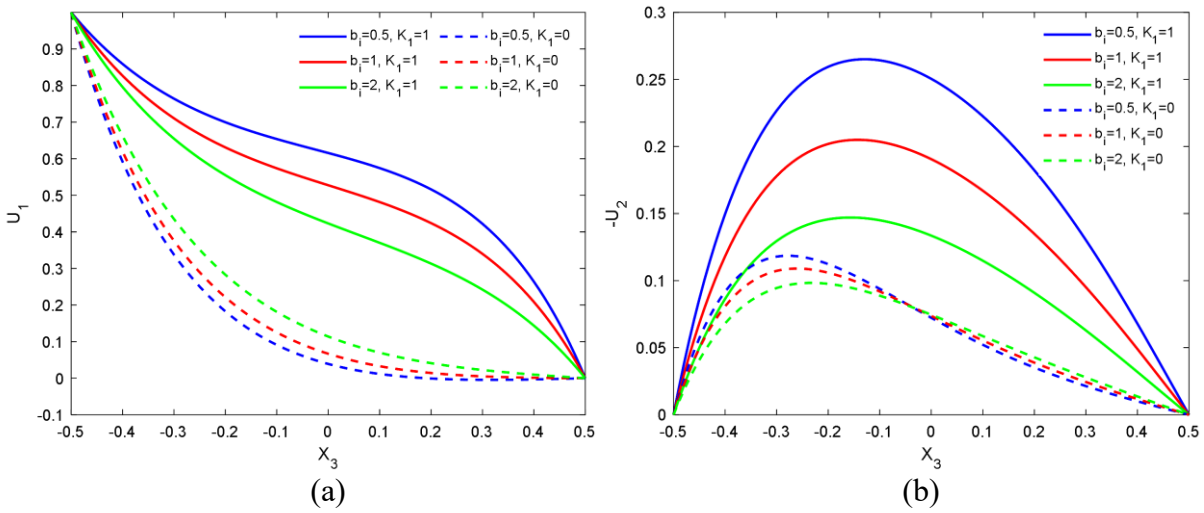

(a) (b)

Figure 9. The effect of ion-slip current (b_i) on the (a) main flow, (b) normal flow.

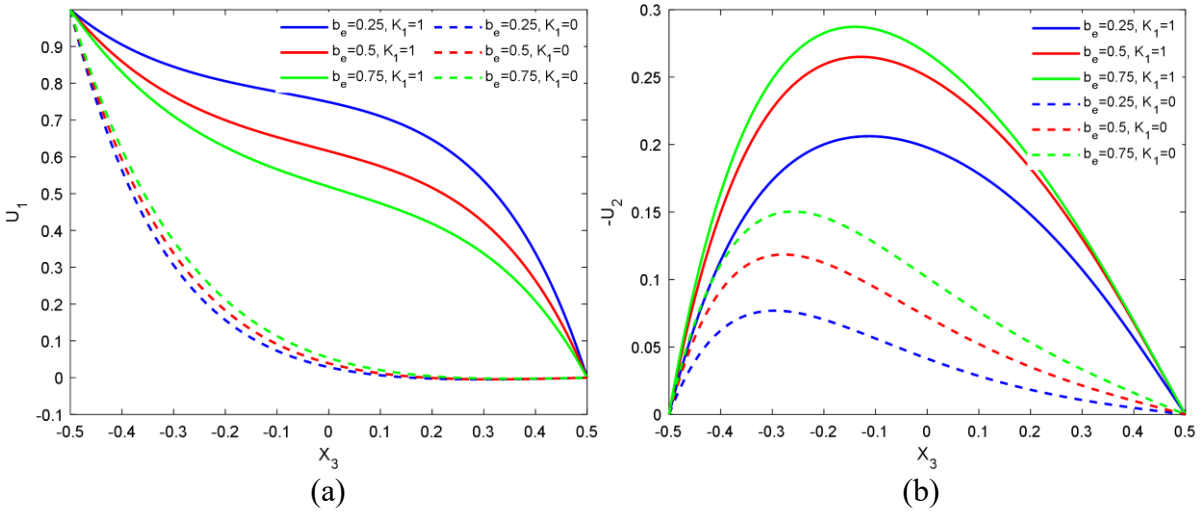

(a) (b)

Figure 10. The effect of Hall current (b_e) on the (a) main flow, (b) normal flow.

Results for quantities of physical interest

The shear stress for the different parameters is displayed in Figures 11 to 18. The impacts of second-grade parameter and rotation on the shear stress are explored in Figures 11 and 12. At the left moving wall, the second-grade parameter and rotation augment the shear stress in the directions of the main and normal flows. On the right wall, the second-grade parameter enhances the shear stress in the direction of the main flow while rotation reduces it due to the centripetal force. The shear stress in the secondary flow direction is diminished by the second-grade parameter for the static magnetic field. This effect is the opposite for the moving magnetic field. Rotation of the system enlarges the shear stress values along the normal flow at the stationary wall. This effect is due to the Coriolis force acting in the direction of the normal flow. Figures 13 and 14 measure the shear stress at the left and right walls respectively for the volume concentration of the nanofluids and Re. At the moving left wall, the shear stress along the main and normal flows is smaller when $\phi_1 = 0.02$ and $\phi_2 = 0.02$ (in the TiO_2-CuO-EO hybrid nanofluid) than when $\phi_1 = 0.02$, $\phi_2 = 0$ (TiO_2-EO nanofluid) and $\phi_1 = 0$, $\phi_2 = 0.02$ (CuO-EO nanofluid). This means that the dispersion of two different types of nanoparticles in the base fluid reduce the shear stress. At

the right static wall, in the case of the moving magnetic field, the shear stress along the main and normal flows is smaller when $\phi_1 = 0.02$ and $\phi_2 = 0.02$ (in the TiO_2-CuO-EO hybrid nanofluid) than when $\phi_1 = 0.02$, $\phi_2 = 0$ (TiO_2-EO nanofluid) and $\phi_1 = 0$, $\phi_2 = 0.02$ (CuO-EO nanofluid). In the case of the static magnetic field, the shear stress along the normal flows is higher when $\phi_1 = 0.02$ and $\phi_2 = 0.02$ (in the TiO_2-CuO-EO hybrid nanofluid) than when $\phi_1 = 0.02$, $\phi_2 = 0$ (TiO_2-EO nanofluid) and $\phi_1 = 0$, $\phi_2 = 0.02$ (CuO-EO nanofluid). At the left wall, the Reynolds number tends to augment the shear stress. On the right wall, in the case of the moving magnetic field, the Reynolds number tends to enhance the shear stress. The effects of the drag due to the permeability of the porous matrix and the presence of the magnetic field on the shear stress are explored in Figures 15 and 16. At the left wall, the shear stress values enlarge for the magnetic drag. The shear stress values along the normal flow reduce while along the main flow rise with the Darcian drag. On the right static wall, the Darcian drag leads to lessen the shear stress. On the right wall, the shear stress values increase with magnetic drag for the moving magnetic field while the opposite trend is observed for the static magnetic field. Figures 17 and 18 present the Hall and ion-slip current's impact on the shear stress. At the right wall, the Hall current leads to an increment in the shear stress along the normal flow and the main flow for the moving magnetic field while the shear stress along the main flow for the static magnetic field has the opposite influence. Ion-slip current leads to a decrement in the shear stress along the normal flow and the main flow for the moving magnetic field while the shear stress along the main flow for the static magnetic field has the reverse feature. At the right wall, the shear stress values decline with the ion-slip current for the moving magnetic field. For the static magnetic field, ion-slip current leads to a rise in the shear stress along the normal flow. The Hall current parameter brings a significant fall in the shear stress along the main flow for the moving magnetic field while it gives significant growth to the shear stress along the normal flow for the static magnetic field. Figure 19 explores, the frequency when $n \geq 2$ and Reynolds number raises the rate of heat transport at the left wall whereas these reduce the rate of heat transport at the right wall. At the left wall, the rate of heat transfer when $\phi_1 = 0.02$ and $\phi_2 = 0.02$ (in the TiO_2-CuO-EO hybrid nanofluid) is smaller than when $\phi_1 = 0.02$, $\phi_2 = 0$ (TiO_2-EO nanofluid) and $\phi_1 = 0$, $\phi_2 = 0.02$ (CuO-EO nanofluid) while at the right wall, this effect is the opposite.

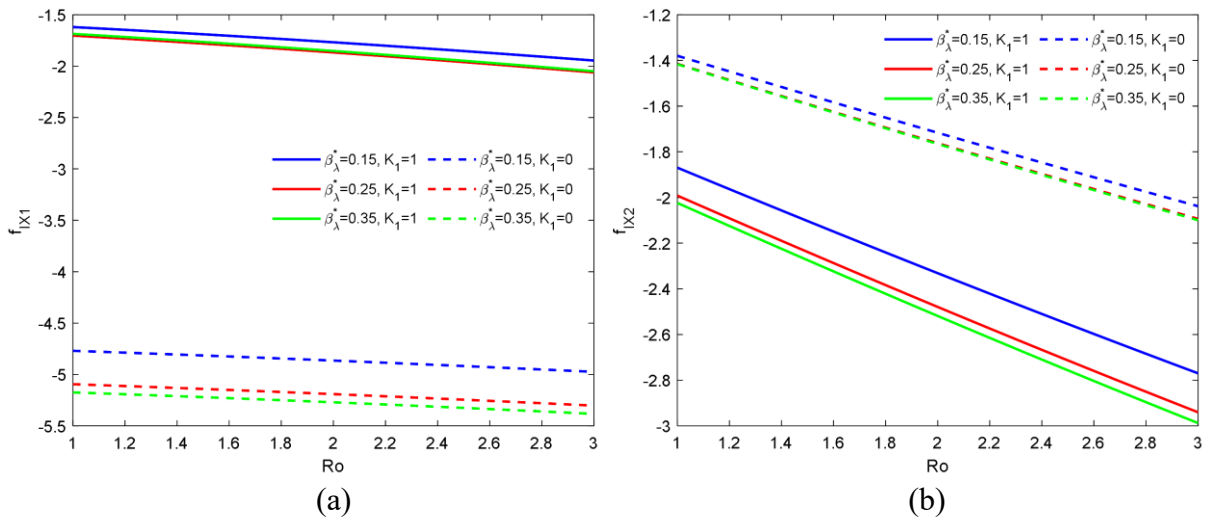

(a) (b)

Figure 11. The effect of the second-grade parameter (β_λ^*) and rotation (Ro) on the shear stress at the left wall along (a) main flow, and (b) normal flow directions.

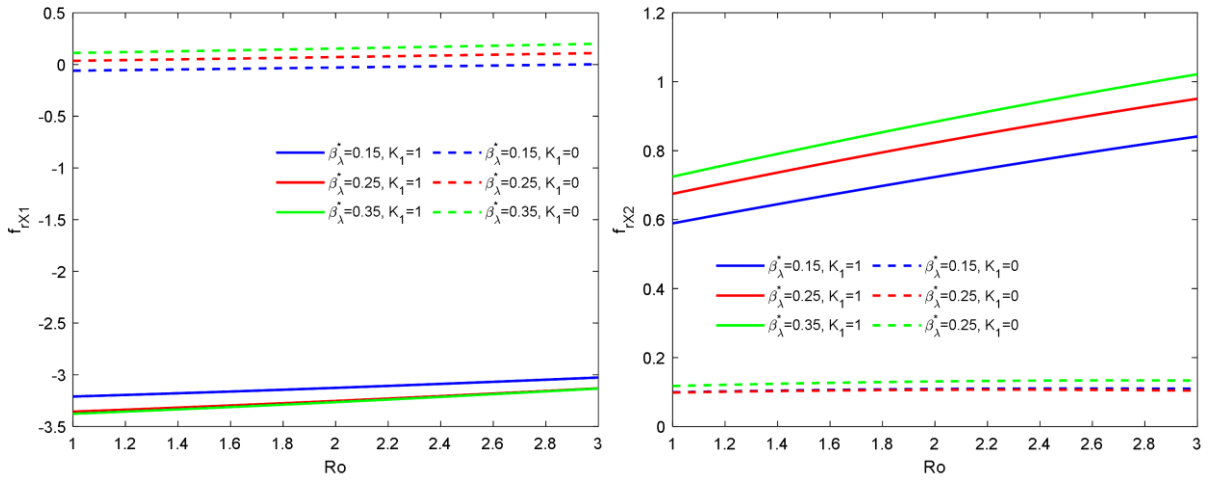

(a) (b)

Figure 12. The effect of the second-grade parameter (β_λ^*) and rotation (Ro) on the shear stress at the right wall along (a) main flow, and (b) normal flow directions.

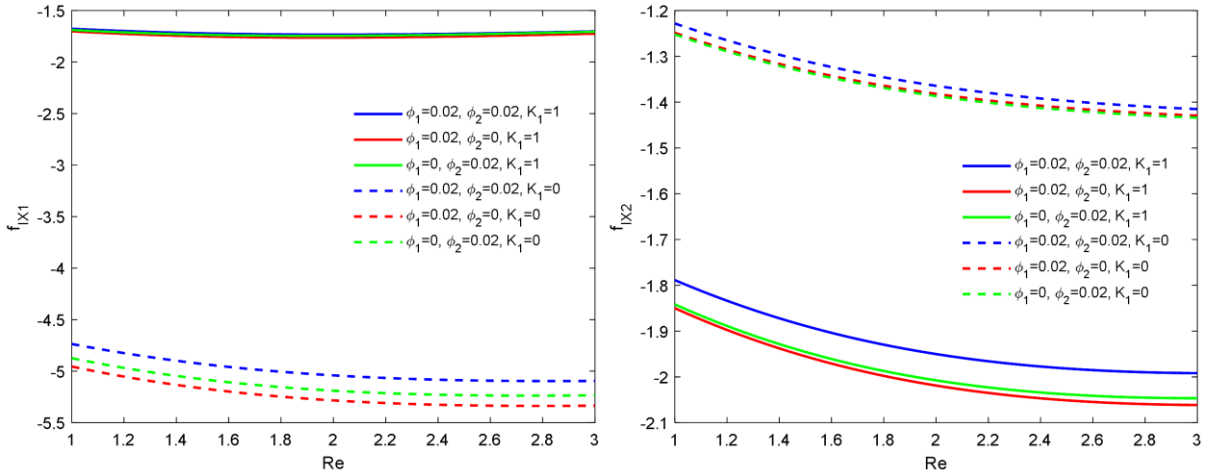

(a) (b)

Figure 13. The effect of Reynolds number (Re) and volume concentrations (ϕ_1 and ϕ_2) on the shear stress at the left wall along (a) main flow, and (b) normal flow directions.

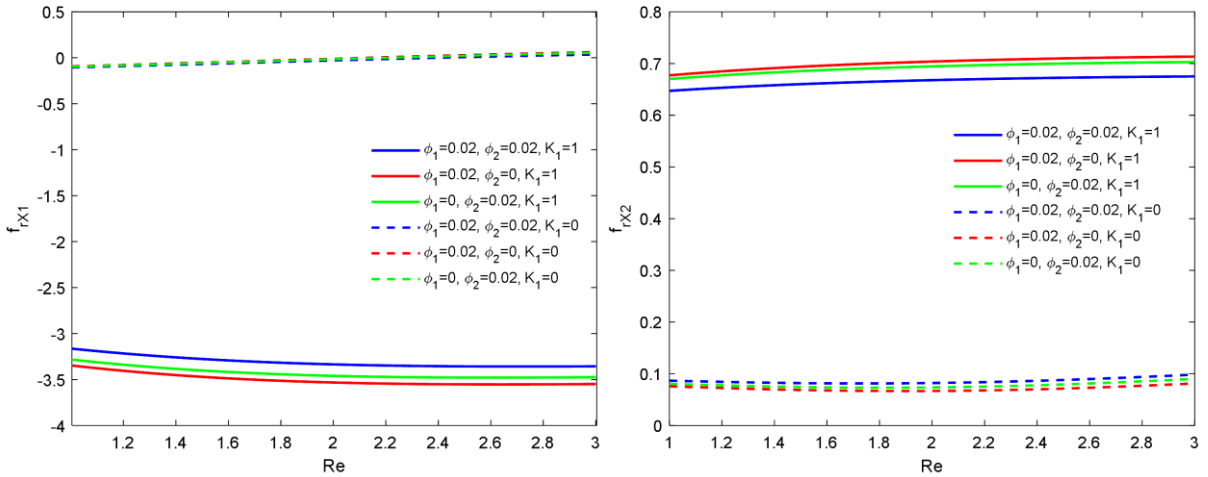

(a) (b)

Figure 14. The effect of Reynolds number (Re) and volume concentrations (ϕ_1 and ϕ_2) on the shear stress at the right wall along (a) main flow, and (b) normal flow directions.

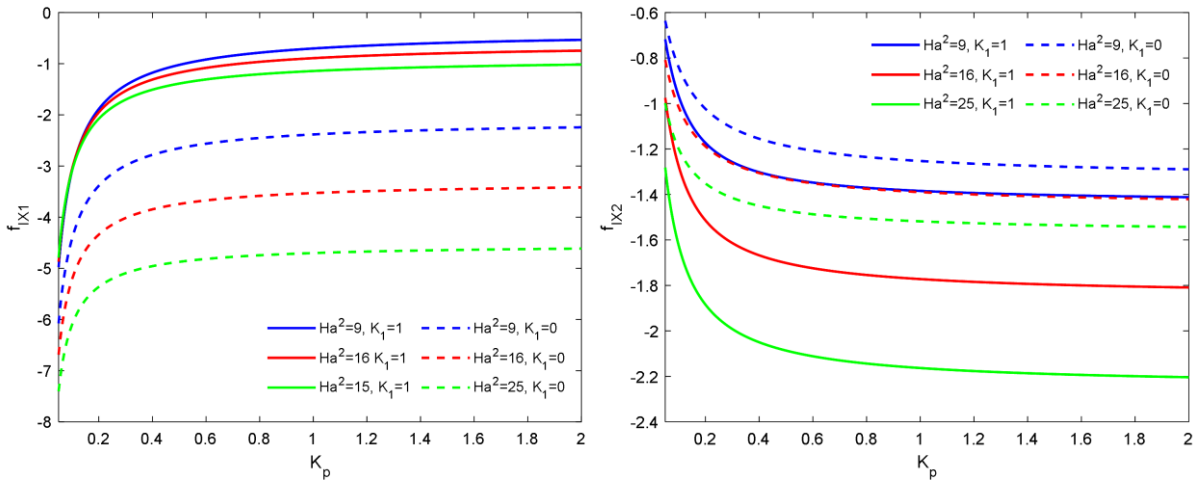

(a) (b)

Figure 15. The effect of the permeability parameter (K_p) and magnetic parameter (Ha^2) on the shear stress at the left wall along (a) main flow, and (b) normal flow directions.

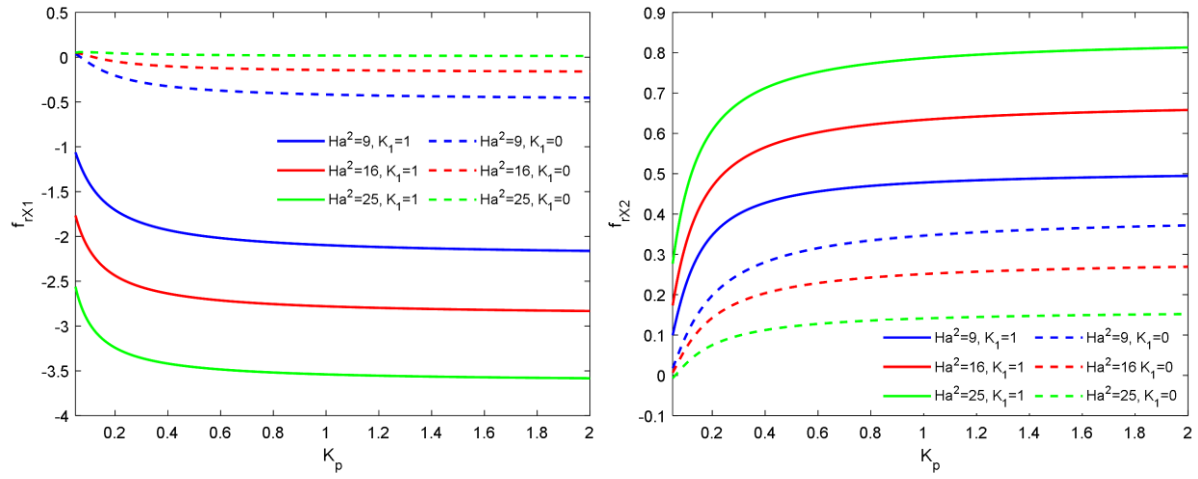

(a) (b)

Figure 16. The effect of the permeability parameter (K_p) and magnetic parameter (Ha^2) on the shear stress at the right wall along (a) main flow, and (b) normal flow directions.

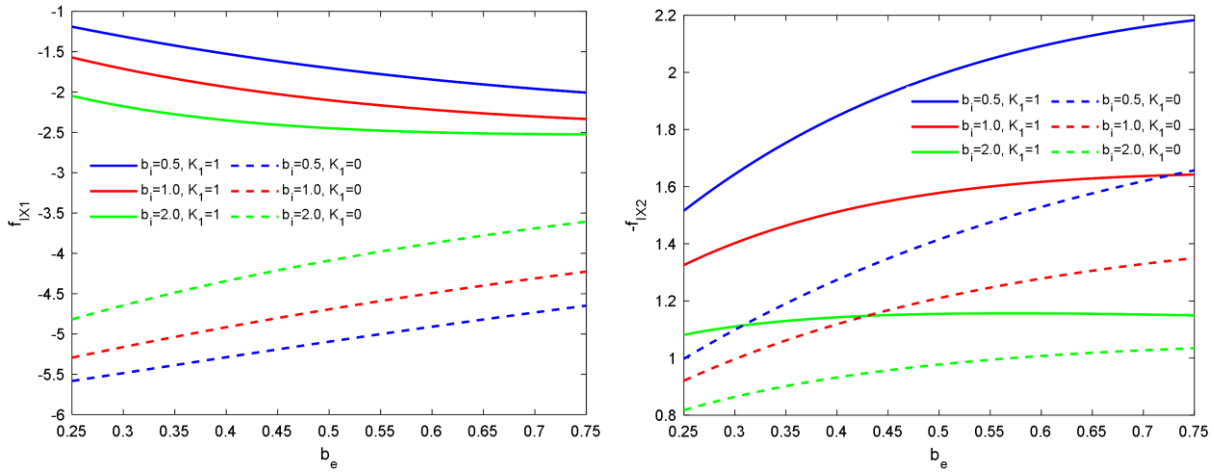

(a) (b)

Figure 17. The effect of Hall current (b_e) and ion-slip current (b_i) on the shear stress at the left wall along (a) main flow, and (b) normal flow directions.

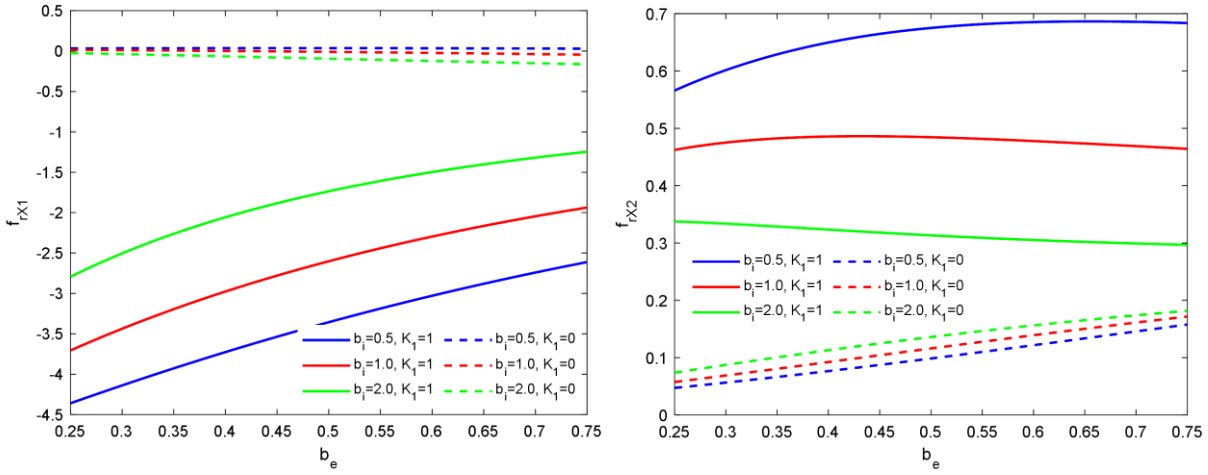

(a) (b)

Figure 18. The effect of Hall current (b_e) and ion-slip current (b_i) on the shear stress at the right wall along (a) main flow, and (b) normal flow directions.

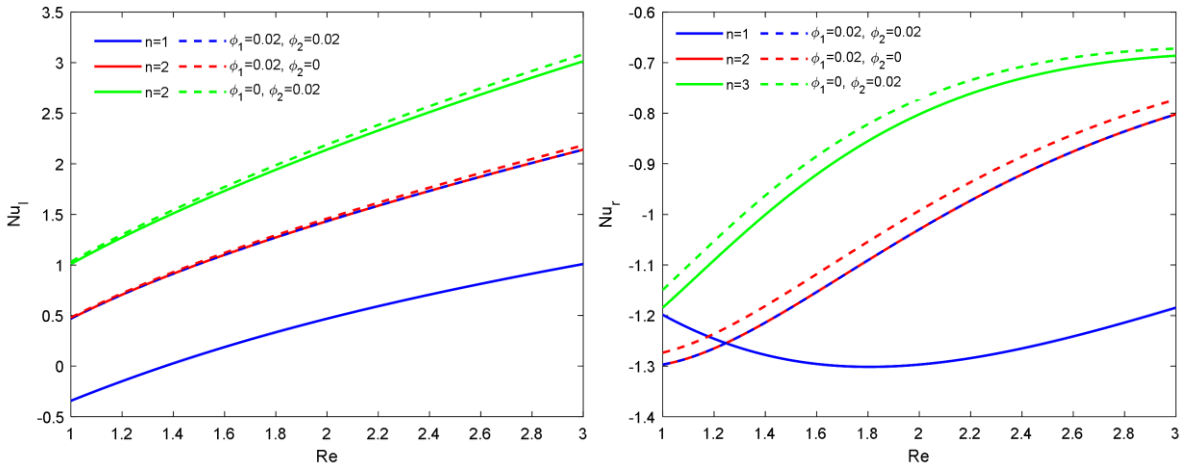

(a) (b)

Figure 19. The effect of Reynolds number (Re) and frequency parameter (n) on the rate of heat transport at the (a) left wall, and (b) right wall.

CONCLUSIONS

This article presents an analytical approach to explore the heat transfer in unsteady hydromagnetic flows of TiO_2-CuO-EO second-grade hybrid nanofluid in a uniform porous matrix bounded by two symmetrically placed vertical walls. The special case of interest is the presence of a moving magnetic field. The flow of a second-grade hybrid nanofluid in a magnetic field has recently been explored in biomedical applications, particularly for targeted drug conveyance. The significant flow characteristics explored are listed below

- The second-grade parameter produces rigidity in the main flow in a stationary magnetic field. In a moving magnetic field, the second-grade parameter employs the flow-assisting force to the main flow. The second-grade parameter also assists the normal flow.
- The static magnetic field suppresses the flow velocity while the moving magnetic field boosts the velocity.
- In a static magnetic field, the velocity in the hybrid nanofluid is higher than the nanofluids. This behaviour is reversed in the moving magnetic field.

- In a static magnetic field, the Hall and ion-slip currents weaken the main flow while in a moving magnetic field, this behaviour is opposite. Both the Hall and ion-slip currents accelerate the normal flow velocity.
- At the left moving wall, the rate of heat transfer in the hybrid nanofluid is smaller than the nanofluid while at the right static wall, this effect is the opposite.

NOMENCLATURE

$\vec{A}_1, \vec{A}_2$	Revlin-Erickson tensor
$\vec{B}$	magnetic field (T)
$\vec{B}_0$	applied magnetic field (T)
b_e	Hall parameter
b_i	ion-slip parameter
C_p	specific heat at constant pressure $(J/kg.K)$
$\vec{e}$	electric field vector
$\left(f_{l_{X_1}}, f_{l_{X_2}}\right)$	shear stress at the left wall along x_1 and x_2 directions
$\left(f_{r_{X_1}}, f_{r_{X_2}}\right)$	shear stress at the right wall along x_1 and x_2 directions
Ro	rotation parameter
$\vec{g}$	acceleration due to gravity (m/s^2)
G_Θ	thermal Grashof number
Ha	magnetic parameter
$\vec{j}$	current density vector (A/m^2)
k	thermal conductivity of the fluid $(W/m.K)$
k_p	permeability of the porous matrix (m^2)
K_p	permeability parameter
Nu_l	rate of heat transport at the left wall
Nu_r	rate of heat transport at the right wall
p	fluid pressure
$\mathbf{Pr}$	Prandtl number
$\mathbf{Re}$	Reynolds number
S	heat source constant
S_1	heat source parameter
t	time (s)
$\vec{T}$	Cauchy stress tensor
T	fluid temperature (K)
T_1	a constant temperature (K)
T_2	a constant temperature (K)
$\vec{u}$	velocity vector
u_0	characteristic velocity (m/s)
(u_1, u_2, u_3)	velocity components (m/s)

(U_1, U_2)	non-dimensional velocity components along x_1 and x_2 directions
x_0	characteristic length
(x_1, x_2, x_3)	rectangular Cartesian coordinates

Greek Symbols

$\alpha_1,\ \alpha_2$	material variables
β_λ	viscoelastic constant
β_λ^*	viscoelastic parameter
ε	constant
μ	dynamic viscosity
υ	kinematic coefficient of viscosity
Ω	angular velocity
ω	oscillation frequency (T^{-1})
ϕ_1	volume concertation of TiO_2-EO nanofluid
ϕ_1	volume concertation of CuO-EO nanofluid
ω	oscillation frequency (T^{-1})
ρ	fluid density (kg/m^3)
σ	electrical conductivity (S/m)
τ	non-dimensional time
Θ	non-dimensional temperature

Subscripts

f	fluid
nf	nanofluid
hnf	hybrid nanofluid
s_1	TiO_2 solute
s_2	CuO solute

Acknowledgment

The author is thankful to the Council of Science and Technology, U. P. (No: CST/D-1527) for financially supporting this research work.

References

[1] ABBAS, W., IBRAHIM, M.A., MOKHTAR, O., MEGAHED, A.M., SAID, A.A. (2023): Numerical analysis of MHD nanofluid flow characteristics with heat and mass transfer over a vertical cone subjected to thermal radiations and chemical reaction. *Journal of Nonlinear Mathematical Physics* **30** (4): 1540–1566. doi: 10.1007/s44198-023-00142-4

[2] ANJALI DEVI, S., SURIYA UMA DEVI, S.S.U. (2016): Numerical investigation of hydromagnetic hybrid Cu–Al2O3/water nanofluid flow over a permeable stretching sheet

with suction. *International Journal of Nonlinear Sciences and Numerical Simulation* **17** (5): 249–257. doi: 10.1515/ijnsns-2016-0037

[3] AFRIDI, M.I., QASIM, M., KHAN, N.A., HAMDANI, M. (2019): Heat transfer analysis of Cu–Al2O3–water and Cu–Al2O3–kerosene oil hybrid nanofluids in the presence of frictional heating: using 3-stage Lobatto IIIA formula. *Journal of Nanofluids* **8** (4): 885–891. doi: 10.1166/jon.2019.1626

[4] BASHIR, S., RAMZAN, M., CHUNG, J.D., CHU, Y.M., KADRY, S. (2021): Analyzing the impact of induced magnetic flux and Fourier's and Fick's theories on the Carreau-Yasuda nanofluid flow. *Scientific Reports* **11** (1): 9230. doi: 10.1038/s41598-021-87831-6

[5] BHATTI, M.M., ÖZTOP, H.F., ELLAHI, R. (2022): Study of the magnetized hybrid nanofluid flow through a flat elastic surface with applications in solar energy. *Materials* **15** (21): 7507. doi: 10.3390/ma15217507

[6] CRAMER, K.R., PAI, S.I. (1973): Magnetofluid Dynamics for Engineers and Applied Physicists. *MacGraw-Hill*, New York.

[7] DAS, A., SAHOO, B. (2018): Flow and heat transfer of a second-grade fluid between two stretchable rotating disks. *Bulletin of the Brazilian Mathematical Society, New Series* **49**: 531–547. doi: 10.1007/s00574-018-0069-9

[8] ENAMUL, S., ONTELA, S. (2024): Magnetohydrodynamic Darcy-Forchheimer flow of non-Newtonian second-grade hybrid nanofluid bounded by double-revolving disks with variable thermal conductivity: Entropy generation analysis. *Hybrid Advances* **6**: 100226. doi: 10.1016/j.hybadv.2024.100226

[9] GUEDRI, K., RAZA, A., KHAN, S.U., KHAN, M.I., SMIDA, K., KUMAR, R.N., GALAL, A.M. (2022): Insight into the dynamics of second-grade fluid subject to inclined magnetic force, newtonian heating, slip flow, and prabhakar-like fractional kind of newtonian heating. *International Journal of Modern Physics B* **36** (25): 2250172. doi: 10.1142/S0217979222501727

[10] GULL, L., MUSTAFA, M., HAQ, R.U. (2024): A novel model for viscoelastic fluid flow and heat near a stretchable plate using variable fluid properties: A computational study. *Numerical Heat Transfer, Part B: Fundamentals* **85 (6)**: 649–661. doi: 10.1080/10407790.2023.2252601

[11] HAQ, S.U., SHAH, S.I.A., JAN, S.U., KHAN, I. (2021): MHD flow of generalized second grade fluid with modified Darcy's law and exponential heating using fractional Caputo-Fabrizio derivatives. *Alexandria Engineering Journal* **60 (4)**: 3845–3854. doi: 10.1016/j.aej.2021.02.038

[12] HAYAT, T., AHMAD, S., KHAN, M.I., ALSAEDI, A. (2017): Non-Darcy Forchheimer flow of ferromagnetic second grade fluid. *Results in physics* **7**: 3419–3424. doi: 10.1016/j.rinp.2017.08.041

[13] HOSSEINZADEH, K., MARDANI, M.R., PAIKAR, M., HASIBI, A., TAVANGAR, T., NIMAFAR, M., GANJI, D.D., SHAFII, M.B. (2023): Investigation of second grade viscoelastic non-Newtonian nanofluid flow on the curve stretching surface in presence of MHD. *Results in Engineering* **17**: 100838. doi: 10.1016/j.rineng.2022.100838

[14] HUANG, J., CHEN, L., LI, S., GUO, J., LI, Y. (2022): Numerical study for the performance of viscoelastic fluids on displacing oil based on the fractional order Maxwell model. *Polymers* **14**: 5381. doi: 10.3390/polym14245381

[15] HUSSAIN, M., IMRAN, M., WAQAS, H., MUHAMMAD, T., ELDIN, S.M. (2023): An efficient heat transfer analysis of MHD flow of hybrid nanofluid between two vertically rotating plates using Keller box scheme. *Case Studies in Thermal Engineering* **49**: 03231. doi: 10.1016/j.csite.2023.103231

[16] HUSSAIN, S., RASHEED, K., ALI, A., VRINCEANU, N., ALSHEHRI, A., SHAH, Z. (2022): A sensitivity analysis of MHD nanofluid flow across an exponentially stretched surface with non-uniform heat flux by response surface methodology. *Scientific Reports* **12** (1): 18523. doi: 10.1038/s41598-022-22970-y

[17] JAMSHED, W., NISAR, K.S., GOWDA, R.P., KUMAR, R.N., PRASANNAKUMARA, B.C. (2021): Radiative heat transfer of second grade nanofluid flow past a porous flat surface: a single-phase mathematical model. *Physica Scripta* **96** (6): 064006. doi: 10.1088/1402-4896/abf57d

[18] JAVAID, M., IMRAN, M., IMRAN, M.A., KHAN, I., NISAR, K.S. (2020): Natural convection flow of a second-grade fluid in an infinite vertical cylinder. *Scientific Reports* **10** (1): 8327. doi: 10.1038/s41598-020-64533-z

[19] KALAIVANAN, R., GANESH, N.V., AL-MDALLAL, Q.M. (2020): An investigation on Arrhenius activation energy of second grade nanofluid flow with active and passive control of nanomaterials. *Case Studies in Thermal Engineering* **22**: 100774. doi: 10.1016/j.csite.2020.100774

[20] KHAN, U., ZAIB, A., ISHAK, A., ALOTAIBI, A.M., ELATTAR, S., POP, I., ABED, A.M. (2022): Impact of an induced magnetic field on the stagnation-point flow of a water-based graphene oxide nanoparticle over a movable surface with homogeneous–heterogeneous and chemical reactions. *Magnetochemistry* **8** (11): 155. doi: 10.3390/magnetochemistry8110155

[21] KOTHANDARAMAN, C.P., SUBRAMANYAN, S. (2010): Heat and mass transfer data book. *New Age International Publishers*.

[22] KUMAR, S., DEO, S., FILIPPOV, A.N. (2022): MHD effects on the flow of second-grade fluid sandwiched between two Newtonian fluid layers through porous medium. *Colloid Journal* **84** (6): 794–805. doi: 10.1134/S1061933X22600099

[23] LI, S., PUNEETH, V., SAEED A.M., SINGHAL, A., AL-YARIMI, F.A., KHAN, M.I., ELDIN, S.M. (2023): Analysis of the Thomson and Troian velocity slip for the flow of ternary nanofluid past a stretching sheet. *Scientific reports* **13** (1): 2340. doi: 10.1038/s41598-023-29485-0

[24] MUHAMMAD, K., HAYAT, T., ALSAEDI, A., AHMAD, B. (2021): Melting heat transfer in squeezing flow of basefluid (water), nanofluid (CNTs+ water) and hybrid nanofluid (CNTs+ CuO+ water). *Journal of Thermal Analysis and Calorimetry* **143**: 1157–1174. doi: 10.1007/s10973-020-09391-7

[25] PUNITH GOWDA, R.J., NAVEEN KUMAR, R., JYOTHI, A.M., PRASANNAKUMARA, B.C., SARRIS, I.E. (2021): Impact of binary chemical reaction and activation energy on heat and mass transfer of marangoni driven boundary layer flow of a non-Newtonian nanofluid. *Processes* **9** (4): 702. doi: 10.3390/pr9040702

[26] RANA, S., NAWAZ, M., ALHARBI, S.O., MALIK, M.Y. (2021): Thermal enhancement in coolant using novel hybrid nanoparticles with mass transport. *Case Studies in Thermal Engineering* **28**: 101467. doi: 10.1016/j.csite.2021.101467

[27] RIVILIN, R. S., ERICKSEN, J. L. (1955): Stress deformation relation for isotropic materials, *Journal of Rational Mechanics and Analysis* **4**: 323–425.

[28] SAKTHI, I., DAS, R., REDDY, P.B.A. (2024a): Entropy generation on MHD flow of second-grade hybrid nanofluid flow over a converging/diverging channel: an application in hyperthermia therapeutic aspects. *The European Physical Journal Special Topics* **233** (6): 1233–1249. doi: 10.1080/10407790.2023.2252600

[29] SAKTHI, I., DAS, R., REDDY, P.B.A. (2024b): Entropy generation analysis on MHD flow of second-grade hybrid nanofluid over a porous channel with thermal radiation. *Numerical Heat Transfer Part B: Fundamentals* **85** (6): 623–648. doi: 10.1080/10407790.2023.2252600

[30] SALAHUDDIN, T., SIDDIQUE, N., KHAN, M., ALTANJI, M. (2022): A significant study on flow analysis of viscoelastic fluid with variable thermo-physical properties. *Mathematics and Computers in Simulation* **194**: 416–429. doi: 10.1016/j.matcom.2021.11.024

[31] SEHRA, S., NOOR, A., HAQ, S.U., JAN, S.U., KHAN, I., MOHAMED, A. (2023): Heat transfer of generalized second grade fluid with MHD, radiation and exponential heating using Caputo–Fabrizio fractional derivatives approach. *Scientific Reports* **13** (1): 5220. doi: 10.1038/s41598-022-22665-4

[32] SHAH, Z., ASGHAR, A., YING, T.Y., LUND, L.A., ALSHEHRI, A., VRINCEANU, N. (2024): Numerical investigation of sodium alginate-alumina/copper radiative hybrid nanofluid flow over a power law stretching/shrinking sheet with suction effect: a study of dual solutions. *Results in Engineering* **21**: 101881. doi: 10.1016/j.rineng.2024.101881

[33] SHAH, N.A., KHAN, I. (2016): Heat transfer analysis in a second-grade fluid over and oscillating vertical plate using fractional Caputo–Fabrizio derivatives. *The European Physical Journal C.*2 **76** (7): 362. doi: 10.1140/epjc/s10052-016-4209-3

[34] SHEIKHOLESLAMI, M., MEHRYAN, S.A.M., SHAFEE, A., SHEREMET, M.A. (2019): Variable magnetic forces impact on magnetizable hybrid nanofluid heat transfer through a circular cavity. *Journal of Molecular Liquids* **277**: 388–396. doi: 10.1016/j.molliq.2018.12.104

[35] SINGH, J.K., HANUMANTHA, KOLASANI, S., HUSSAIN, S.M. (2023b): Exploration of heat and mass transport in oscillatory hydromagnetic nanofluid flow within two verticals alternatively conducting surfaces. *ZAMM-Journal of Applied Mathematics and Mechanics* **103** (12): e202300216. doi: 10.1002/zamm.202300216

[36] SINGH, J.K., JOSHI, N., ROHIDAS, P. (2018): Unsteady MHD natural convective flow of a rotating Walters'-B fluid over an oscillating plate with fluctuating wall temperature and concentration. *Journal of Mechanics* **34** (4): 519–532. doi: 10.1017/jmech.2017.25

[37] SINGH, J.K., KOLASANI, S. (2021): Energy dissipation and Hall effect on MHD convective flow of nanofluid within an asymmetric channel with arbitrary wall thickness and conductance. *The European Physical Journal Plus* **136** (10): 1074. doi: 10.1140/epjp/s13360-021-02022-6

[38] SINGH, J.K., KOLASANI, S., HANUMANTHA, SETH, G.S. (2023a): Scrutiny of induced magnetic field and Hall current impacts on transient hydromagnetic nanofluid flow within two vertical alternative magnetized surfaces. *Proceedings of the Institution of Mechanical Engineers, Part E: Journal of Process Mechanical Engineering* **237** (4): 1595–1606. doi: 10.1177/09544089221119255

[39] SINGH, J.K., KOLASANI, S., SETH, G.S. (2024): Heat and mass transport nature of MHD nanofluid flow over a magnetized and convectively heated surface including Hall current, magneto and thermo diffusions impacts. *Ricerche di Matematica* **73** (3): 1537–1557. doi: 10.1007/s11587-022-00687-4

[40] SINGH, J.K., SETH, G.S. (2022): Heat and mass transport performance of MHD elastico-viscous fluid flow over a vertically oriented magnetized surface with magnetic and thermo diffusions. *Heat Transfer* **51** (2): 2258–2278. doi: 10.1002/htj.22399

[41] SINGH, J.K., SETH, G.S., BEGUM, G. (2020): Hydromagnetic free convective flow of Walters'-B fluid over a vertical surface with time-varying surface conditions. *World Journal of Engineering* **17** (2): 295–307. doi: 10.1108/WJE-06-2019-0163

[42] SINGH, J.K., SETH, G.S., HUSSAIN, S.M. (2023c): Thermal performance of hydromagnetic nanofluid flow within an asymmetric channel with arbitrarily conductive walls filled with Darcy-Brinkman porous medium. *Journal of Magnetism and Magnetic Materials* **582**: 171034. doi: 10.1016/j.jmmm.2023.171034

[43] SINGH, J. K., VISHWANATH, S. (2020): Hall and ion-slip effects on MHD free convective flow of a viscoelastic fluid through porous regime in an inclined channel with moving magnetic field. *Kragujevac Journal of Science* **42**: 5–18.

[44] SRAVAN KUMAR, T., DINESH, P.A., MAKINDE, O.D. (2020): Impact of Lorentz force and viscous dissipation on unsteady nanofluid convection flow over an exponentially moving vertical plate. *Mathematical Models and Computer Simulations* **12**: 631–646. doi: 10.1134/S2070048220040110

[45] SRINIVASA, C.T., SINGH, J.K., GIREESHA, B.J. AND ARCHANA, M. (2019): Effect of variable fluid properties on Magnetohydrodynamic flow of nanofluid past a flat plate. *Journal of Nanofluids* **8** (3): 520–525. doi: 10.1166/jon.2019.1608

[46] SREEDEVI, P., REDDY, P.S. (2022): Effect of magnetic field and thermal radiation on natural convection in a square cavity filled with TiO2 nanoparticles using Tiwari-Das nanofluid model. *Alexandria Engineering Journal* **61** (2): 1529–1541. doi: 10.1016/j.aej.2021.06.055